A New Coarse-to-Fine Framework for 3D Brain MR Image Registration

Terrence Chen[1], Thomas S. Huang[1], Wotao Yin[2], and Xiang Sean Zhou[3]

[1] University of Illinois at Urbana Champaign,
Urbana, IL 61801, USA
{tchen5, huang}@ifp.uiuc.edu
[2] Columbia University,
New York, NY, USA
wy2002@columbia.edu
[3] Siemens Corporate Research,
Princeton, NJ 08540, USA
xzhou@scr.siemens.com

Abstract. Registration, that is, the alignment of multiple images, has been one of the most challenging problems in the field of computer vision. It also serves as an important role in biomedical image analysis and its applications. Although various methods have been proposed for solving different kinds of registration problems in computer vision, the results are still far from ideal when it comes to real world biomedical image applications. For instance, in order to register 3D brain MR images, current state of the art registration methods use a multi-resolution coarse-to-fine algorithm, which typically involves starting with low resolution images and working progressively through to higher resolutions, with the aim to avoid the local maximum "traps". However, these methods do not always successfully avoid the local maximum. Consequently, various rather sophisticated optimization methods are developed to attack this problem. In this paper, we propose a novel viewpoint on the coarse-to-fine registration, in which coarse and fine images are distinguished by different scales of the objects instead of different resolutions of the images. Based on this new perspective, we develop a new image registration framework by combining the multi-resolution method with novel multi-scale algorithm, which could achieve higher accuracy and robustness on 3D brain MR images. We believe this work has great contribution to biomedical image analysis and related applications.

1 Introduction

In medical image analysis, what is most often desired is a proper integration of the information provided by different images. Image registration, serving as the first step of the information integration process, is to bring various images into spatial alignment. In other words, it is a process of overlaying multiple images of the same type of objects taken at different times, by different modalities, and from different subjects. Image registration serves various functions in medical image applications: it can be used to obtain ampler information about the patient by registration images acquired from different modalities, to monitor and investigate tumor growth by images taken at

Y. Liu, T. Jiang, and C. Zhang (Eds.) CVBIA 2005, LNCS 3765, pp. 114 – 124, 2005.

different times, to compare patients' data with anatomical atlases, to correct the motion of a series of data acquired continuously, etc. Despite the fact that registration is of great significance, fully automatic registration with high accuracy and robustness on 3D data is hardly achieved due to the difficulties of finding the most proper settings of the following factors: transformation, interpolation, similarity metric, and optimization. In this paper, we propose a multi-scale and multi-resolution coarse-to-fine (MMCTF) optimization method for 3D brain MR image registration, which can be used in conjunction with any transformation, interpolation method, and similarity metric to obtain consistent and accurate registration results.

1.1 Issues in Brain MRI Registration

In this section, we briefly introduce existing methods for medical image registration. A survey of more medical image registration methods, including semi-automatic registration methods using landmarks and interactive registration, can be found in [9]. Registration is the process to seek a transformation $T(\cdot)$ that registers the floating image F and the reference image R by maximizing their similarity:

$$T = \arg\max_T S(T(F(x)), R(x)), \tag{1}$$

where x are the coordinates of the voxel, and S is the similarity metric which measures the closeness of the two images. Determining the type of transformation is the first task of registration. It can be divided into linear transformation and nonlinear warping. Considering 3D linear transformation, it can be from 6 DOF (a rigid body transformation including 3 translations and 3 rotations) up to 12 DOF (an affine transformation including 3 translations, 3 rotations, 3 scales, and 3 skew parameters). Nonlinear warping encompasses a wide range of transformations, which can be up to millions of DOF and allow any geometric change between images. The most suitable type of transformation is determined based on factors such as the characteristics of the data, the need of a specific experiment or application, the dimensionality and the size of the data, and the tradeoff between speed and accuracy.

Interpolation methods are used to calculate the intensity of location between discrete points during transformation. There are several widely-practiced interpolation methods. Nearest neighbor decides the intensity of a location by taking the value from its nearest neighbor. Trilinear interpolation calculates the intensity from the 8 corner points of the 3D cube encompassing the specific location. Sinc interpolation calculates local intensity from much more than 8 neighbors. Although it is generally more accurate for registration between images with large transformations, Sinc interpolation requires much more computational time and is not widely used in 3D data.

Selecting the similarity metric is one of the most challenging problems in medical image analysis. Its purpose is to measure the closeness of different images. Similarity measurements of intra-modal and inter-modal registration of two images may be very different. In practice, mean absolute difference, least square difference, and normalized correlation are often used for intra-modal registration whereas mutual information [19], woods [20], and correlation ratio [16] are suitable for inter-modal cases.

Optimization method is used to search for the transformation that maximizes the similarity value given the cost function and the type of transformation. Although global maximum is always desired, it is not always worth doing exhaustive search due

to unacceptable computational overhead, especially when the search is performed in high dimensional space. Powell's method [15] and gradient descent are two of the most well-known and widely-used local optimization methods. Multi-resolution methods, on the other hand, are often used to improve the robustness and speed up the registration process. A multi-resolution method is a coarse-to-fine method where images are registered progressively through lower resolutions to higher resolutions. Different resolutions of the image are obtained by different sub-samplings (fig. 2 (I)). Other optimization methods include apodization of the cost function [6], multi-start, etc. Apodization of the cost function gives greater weighting to the object region inside the FOV (Filed of View). Multi-start obtains several local maximums during the lowest resolution match and then passes these candidates to the next level to reduce the chance of missing the global maximum.

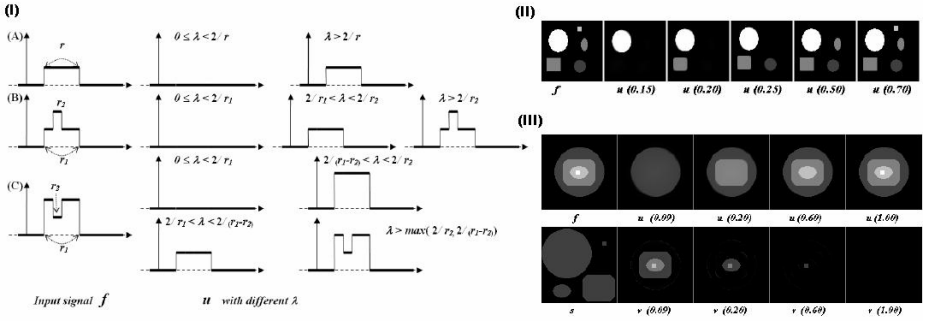

Fig. 1. (I) The TV-$\mathcal{L}^1$-model on 1-d signal. Note that small scale signal can be separated from large scale signal using different λ according to their scale r▷ ←—*II*— Original image f and different level of u when applying different (λ). (III) Additive signals with one included in the other can be extracted one by one using increasing values of (λ). s shows the original intensities of the four shapes before addition.

2 Methodology

In this section, we introduce the MMCTF framework and illustrate how it works for image registration. Before that, we first introduce the TV-L^1 model and extend it to 3D, which serves as the basis of the proposed framework. In the TV-based framework, an image f is modeled as the sum of image cartoon u and texture v, where f, u and v are defined as functions (or flow fields) in appropriate spaces. Cartoon contains background hues and important boundaries as sharp edges. The rest of the image, which is texture, is characterized by small-scale patterns. Since cartoon u is more regular than texture v, we can obtain u from image f by solving:

$$\min \int_{\Omega} |\nabla u| + \lambda \| t(u, f) \|_B, \tag{2}$$

where $\int_\Omega |\nabla u|$ is the total variation of u over its domain Ω, $\|t(u, f)\|_B$ can be any measure of the closeness between u and f, and λ is a scalar weight parameter. The choice of

the measure $\|\cdot\|_B$ depends on applications. The first use of this model was the ROF model for image denoising [17], where $\|t(u, f)\|_B = \|f - u\|_{L^2}$. The essential merit of total variation based image model is the edge-preserving property [18]. First, minimizing the regularization measure $\int_\Omega |\nabla u(x)| dx$ only reduces the total variation of u over its support, a value that is independent of edge smoothness. Second, unless $\|t(u, f)\|_B$ specifically penalizes sharp edges, minimizing a fidelity term $\|t(u, f)\|_B$ (e.g., L^1 or L^2-norm of $f - u$) generally tends to keep u close to f, and thus, also keeps edges of f in u. Finally, minimizing $\int_\Omega |\nabla u| + \lambda \|t(u, f)\|_B$, with λ sufficiently big will keep sharp edges. ROF uses the L^2-norm, which penalizes big point-wise differences between f and u, so it removes small point-wise differences (noise) from f. Mainly due to this good edge-keeping property, this model has been adopted, generalized and extended in many way. One of them uses the L^1-norm as the fidelity term [2, 3, 11].

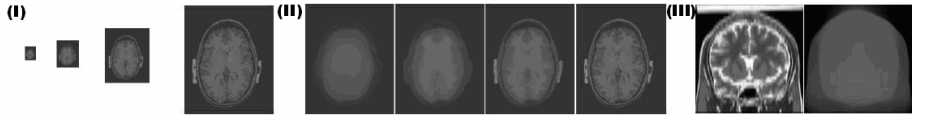

Fig. 2. (I) Traditional coarse-to-fine method uses different sub-samplings of the images. (II) Multi scales of the brain image obtained by the TV-L^1 model. (III) The contour image obtained by 3D TV-L^1 model (right) does not contain artifacts or noise in the original image (left).

2.1 The TV-L^1 Model for Scale-Driven Image Extraction

Formally, this TV-L^1 model is formulated as:

$$\min \int_\Omega |\nabla u(x)| dx \qquad s.t. \| f(x) - u(x) \|_{L^1} \le \sigma, \tag{3}$$

where Ω is the image domain where functions f and u are defined on. Since (3) is a convex optimization problem, it can be reformulated as

$$\min_u \int_\Omega |\nabla u(x)| dx + \lambda | f(x) - u(x) | dx, \tag{4}$$

Just like the L^2-norm, the L^1-norm keeps u close to f (but under a different measure), so the edge-preserving property can be easily seen by following the similar argument of the ROF model. To concrete our claims, we give the TV-L^1 analytical results of some easy problems from $\mathfrak{R}$ to $\mathfrak{R}^3$. Fig.1 (I) illustrates the TV-L^1 method applied to 1-d signal. According to fig. 1 (I), with different values of λ, u keeps different signals according to their scales but not intensities. Now, we extend this to 2-d signal (i.e. an image). Chan and Esedoglu [3] have proved that solving equation (4) is equivalent to solving the following level-set-based geometrical problem:

$$\min_u \int_{-\infty}^{+\infty} Per(\{x : u(x) > u\}) + \lambda Vol(\{x : u(x) > u\} \oplus \{x : f(x) > u\}) du, \tag{5}$$

where $Per(\cdot)$ is the perimeter function, $Vol(\cdot)$ is the volume function, and $S1 \oplus S2 := (S1 \backslash S2) \cup (S2 \backslash S1)$, for any set $S1$ and $S2$. Using equation (5), Chan and Esedoglu [3] proved the following geometric properties of the solution $v(\lambda) = f - u(\lambda)$ in (4):

• Suppose $f = c_1 1_{Br(y)}(x)$, a function with the intensity c_1 in the disk centered at y and with radius r, and the intensity 0 anywhere else. Then

$$u(\lambda) = \begin{cases} 0 \quad , & 0 \le \lambda \le 2/r \\ \{s 1_{B_r(y)}(x) : 0 \le s \le c_1\} \quad , & \lambda = 2/r \\ c_1 1_{B_r(y)}(x) \quad , & \lambda > 2/r \end{cases} \tag{6}$$

By this property, when applying different values of λ, objects of different scales can be kept in either u or v. Fig. 1 (II) illustrates this property. Furthermore, we can extend this property to the following:

• Suppose $f = c_1 1_{Br_1}(y)(x) + c_2 1_{Br_2}(y)(x)$, where $0 < r_2 < r_1$ and $c_1, c_2 > 0$.

$$u(\lambda) = \begin{cases} 0 \quad , & \lambda < 2/r_1 \\ c_1 1_{B_{r_1}(y)}(x) \quad , & 2/r_1 < \lambda < 2/r_2 \\ (c_1 1_{B_{r_1}(y)} + c_2 1_{B_{r_2}(y)})(x) \quad , & \lambda > 2/r_2 \end{cases} \tag{7}$$

Fig. 1 (III) illustrates this property, which is proved in [4]. More discussions on 2D properties of the TV-L^1 model can be found in [21].

2.2 3D TV-ψ-Model

The properties discussed in the previous section which has been developed and used for 2D image can be simply extended to 3D. First, we extend property (5) and claim that solving (2) in 3D is equal to solve the following equation:

$$\min_u \int_{-\infty}^{+\infty} Sur(\{x : u(x) > u\}) + \lambda Vol(\{x : u(x) > u\} \oplus \{x : f(x) > u\}) du, \tag{8}$$

where $Sur(\cdot)$ is the surface area function, and $Vol(\cdot)$ is the volume function. Using equation (8), we can extend previous geometric properties (6) and (7) to:

• Suppose $f = c_1 1_{Br}(y)(x)$, a function with the intensity c_1 in the ball centered at y and with radius r, and the intensity 0 anywhere else. Then

$$u(\lambda) = \begin{cases} 0 \quad , & 0 \le \lambda \le 3/r \\ \{s 1_{B_r(y)}(x) : 0 \le s \le c_1\} \quad , & \lambda = 3/r \\ c_1 1_{B_r(y)}(x) \quad , & \lambda > 3/r \end{cases}, \tag{9}$$

• Suppose $f = c_1 1_{Br1}(y)(x) + c_2 1_{Br2}(y)(x)$, where $0 < r_2 < r_1$ and $c_1, c_2 > 0$. Then

$$u(\lambda) = \begin{cases} 0 \quad , & \lambda < 3/r_1 \\ c_1 1_{B_{r_1}(y)}(x) \quad , & 3/r_1 < \lambda < 3/r_2 \\ (c_1 1_{B_{r_1}(y)} + c_1 1_{B_{r_2}(y)})(x) \quad , & \lambda > 3/r_2 \end{cases}, \tag{10}$$

(9) is proved as follows and (10) can be easily proved by following the proof of (7).

Proof of property (9):
Proof. By assumption, $f = c11Br(y)(x)$. Without loss of generality, we assume $c_1 > 0$. Clearly, solution $u(x)$ of (4) is bounded between 0 and c_1, for all $x \in \Omega$. It follows that (8) is simplified to:

$$\min_u \int_0^{c_1} Sur(\{x : u(x) > u\}) + \lambda Vol(\{x : u(x) > u\} \oplus \{x : f(x) > u\})du, \tag{11}$$

Since $\{x : f(x) > u\} \equiv Br(y)$ for $u \in (0; c_1)$, $S(u) := \{x : u(x) > u\}$ must solve the following geometry problem:

$$\min_S Sur(S(u)) + \lambda Vol(S(u) \oplus B_r(y)), \tag{12}$$

for almost all $u \in (0; c_1)$. First, $S(u) \subseteq Br(y)$ holds because, otherwise, $S(u) := S(u) \cap Br(y)$ achieves lower objective value than $S(u)$. Then, it follows that

$$Vol(S(u) \oplus B_r(y)) = Vol(B_r(y) \setminus S(u)) \tag{13}$$

Therefore, to minimize (12) is to minimize the surface area of S while maximizing its volume. By extending the Isoperimetric Theorem into 3D, $S(u)$ must be either empty or a ball. Let r_S denote the radius of S, it follows that $r_S = r$ if $\lambda > 3/r$, $r_S = 0$ if

$0 \le \lambda < 3/r$, and r_S ({0, r} if = 3/r. ■

Based on the above properties, we can extract different scales of a brain by different λs, which is illustrated in fig. 2 (II). More precisely, if we select $\lambda \approx 3/r$, where r is close to the radius of the brain region, u will be close to the 3D contour of the brain.

2.3 The MMCTF Registration Algorithm

Traditional 3D brain MRI registration methods avoid local minimum and improve the efficiency of the registration process by a multi-resolution coarse-to-fine algorithm. This approach is not always sufficient for avoiding local minimum traps. To overcome this limitation, we propose a new viewpoint on coarse-to-fine registration – coarse and fine images can be distinguished by different scales of the objects (fig. 2 (II)). However, if we do a pure multi-scale coarse-to-fine registration, it may lose the efficiency of the traditional multi-resolution method. Hence, instead of using multi-scale method only, we develop a novel framework combining the two methods together to avoid the limitation of each other. Fig. 3 illustrates our final algorithm, a Multi-scale and Multi-resolution Coarse-To-Fine (MMCTF) framework. In order to simplify following discussions, we call the u obtained using $\lambda \approx 3/r$, which is the largest scale we used in the MMCTF framework, the *contour image* in this paper. In the MMCTF algorithm, the first step is to obtain the *contour images* of both the floating image and the reference image using 3D TV-L^1 model with λ (3/r, where r is the radius specifying the volume of interest. Second, we use a traditional coarse-to-fine (multi-resolution) method to register the two contour images. An initial search for translation, rotation, and global scaling parameters is applied at the beginning of the lowest resolution registration to speed up the search. The initial search includes matching the COM (center of mass) of the two images and finding the best initial rotation by searching every 30 degree in all directions. Since it is in the lowest resolu-

tion, this initial search can be done efficiently. After the initial search, the Powell's local optimization method [15] is used to search for the maximum of the similarity measurement in each level. Followed by the registration of the contour images, the final parameters can be used to register the floating and reference images. We would like to point out that although we can do more scales in between the contour image and the original image by increasing the value of ((fig. 2 (II)), empirically only two scale levels are enough for robust and accurate registration. Besides, it is much more efficient to perform the registration with only two scale levels. There are several advantages of this combination framework: 1.) The multi-resolution method is used for initial registration, which finds a good registration efficiently at the beginning. 2.) Since the multi-resolution is performed on the contour images, which consist of only the contours without detailed features, the chance that the gross features in the low resolution images mislead further registration is much smaller. 3.) By a multi-scale registration, a good registration can be easily found based on the contour images. 4.) Noise or other artifacts, which may degrade the registration performance and cause local maximum/minimum, barely exist in the contour images. (fig. 2 (III)) 5.) Empirically, only two scale levels are enough to obtain satisfying results. Besides, since the registration of the contour images is mostly very close to the final registration, step 10 in fig. 3 normally costs only a little more computational time than pure multi-resolution method.

1. $F^1 \leftarrow$ Normalize(input floating image)
2. $R^1 \leftarrow$ Normalize(reference image)
3. $F_c^1 \leftarrow \arg\min_u \int_\Omega |\nabla u(x)| + \frac{3}{r_F}|F(x) - u(x)|\, dx$
4. $R_c^1 \leftarrow \arg\min_u \int_\Omega |\nabla u(x)| + \frac{3}{r_R}|R(x) - u(x)|\, dx$
5. $\Theta \leftarrow$ calculate initial parameters based on F_1^8 and R_1^8
6. $\Theta \leftarrow \arg\max_\Theta$ Registration(F_c^8, R_c^8, Θ)
7. $\Theta \leftarrow \arg\max_\Theta$ Registration(F_c^4, R_c^4, Θ)
8. $\Theta \leftarrow \arg\max_\Theta$ Registration(F_c^2, R_c^2, Θ)
9. $\Theta \leftarrow \arg\max_\Theta$ Registration(F_c^1, R_c^1, Θ)
10. $\Theta \leftarrow \arg\max_\Theta$ Registration(F^1, R^1, Θ)
11. Output $\leftarrow$ Transformation(F^1, Θ)

F^i: sub-sampling of F to i mm in thickness.
r_F: radius of the brain in image F.
r_R: radius of the brain in image R.
I_c: the *contour image* of image I.
Normalize($\cdot$): normalize image to 1mm in thickness.
Registration(A, B, Θ): Register A to B by parameter set Θ.
Transformation(A, Θ): Transform A by parameter set Θ.

Fig. 3. The MMCTF algorithm

3 Experimental Results

In this section, we compare the proposed MMCTF algorithm with one of the famous brain MR image registration methods, FLIRT [6], and with the traditional pure multi-resolution (PMR) coarse-to-fine method. For fair comparison, the following settings are used in all methods throughout the experiments. Transformation: 3D affine transformation with 12 DOF (3 translations, 3 rotations, 3 scales, and 3 skews). Cost function: although any similarity metric can be used in our framework, correlation ratio is adopted for inter-modal registration since it is suggested in [6], which we aim to compare to. In addition, normalized correlation is used for intra-modal registration. Interpolation: Trilinear interpolation. The step sizes used to search for each parameters are: translation: $\Delta t = 0.5$, rotation: $\Delta\theta = 0.3°$, scale: $\Delta s = 0.005$, and skew: $\Delta k = 0.005$. The number of intensity bins used per image for correlation ratio is $256/n$, where n is the resolution in *mm*. Some other optimization settings used by FLIRT (i.e. apodization of

the cost function, multi-start, etc.) to improve robustness and efficiency are not implemented in PMR and MMCTF. The T_1 weighted images we use are real 3D brain MR images. The T_2 weighted image is obtained from brainweb [8].

3.1 Accuracy Evaluation

Although the quantitative assessment of registration methods is quite difficult, a method can be affirmed as relatively more accurate than others if it consistently obtains higher similarity values, under the circumstances that all other settings are the same. In the first experiment, we evaluate the registration accuracy between 6 high resolution T_1 weighted MR images with size 207×255×207. 15 total registrations between each pair of the six images are evaluated. Normalized correlation is chosen as the similarity measurement. Fig. 4 shows the results. In fig. 4, the three methods achieve similar and consistent results, which means that the traditional multi-resolution method is good enough for high resolution intra-modal registration. Next, we evaluate the inter-modal registration accuracy between images with different resolution. In this experiment, we register one low resolution 181×217×30, T_2 weighted MR image with voxel dimension 1×1×5 mm^3 to six different high resolution 207×255×207, T_1 weighted MR images with voxel dimension 1×1×1 mm^3. Correlation ratio is used to measure the similarity. Fig. 5 illustrates the results. In this more complicated and difficult case, although all methods register the images well, the strength of MMCTF is demonstrated by the higher similarity of images. Fig. 5 shows that the MMCTF algorithm reaches higher maximum value of the correlation ratio, which proves that the proposed algorithm has a much higher chance to reach global

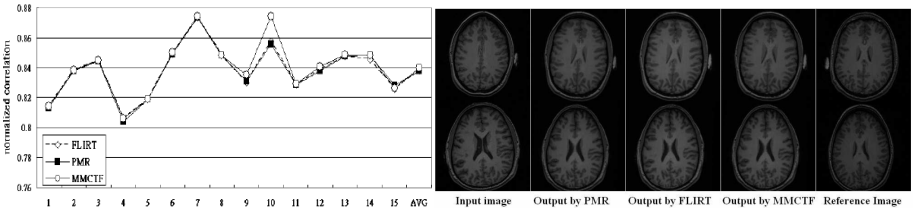

Fig. 4. Left: Normalized correlation between registered and reference images (intra-modal registration). Right: An example (2D slice from 3D data).

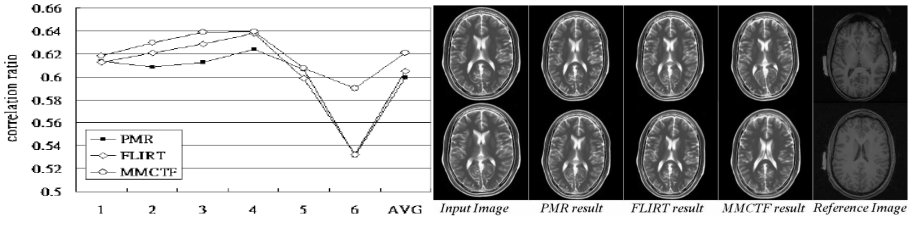

Fig. 5. Left: Correlation ratio between registered and reference images (inter-modal registration). Right: An example (2D slice from 3D data).

maximum. It can also be observed by human eyes that the registration results of the MMCTF are closer to the reference images (fig. 5 (right)).

3.2 Robustness Evaluation

The robustness evaluation of the registration method is originally purposed by Jenkinson and Smith [7]. In this paper, we use a similar way to evaluate the robustness of the registration algorithm. Similar to the inter-modal experiment in the accuracy evaluation, we register the same low resolution T_2 weighted MR image with voxel dimension 1×1×5 mm^3 to six different high resolution T_1 weighted MR images with voxel dimension 1×1×1 mm^3. However, for each registration, we operate ten different initial transformations on the T_2 weighted low resolution image before the registration process, including four global scalings of 0.7, 0.8, 0.9, and 1.1, four different rotations of -10, -2, 2, and 10 degrees about the anterior-posterior (y) axis, and two extreme cases with rotations of -10 and 10 degrees about y axis plus the second skew factor = 0.4. The ten transformed images are then registered to the reference image. To evaluate the robustness, we compare the ten registration results to the registered image which obtained directly from the original floating image to the reference image. If the registration algorithm is robust, these 10 values should show little difference. Fig. 6 shows the results. In fig. 6 (I), the variance between the results obtained by the MMCTF model is much smaller than the variances of FLIRT and PMR. In fact,

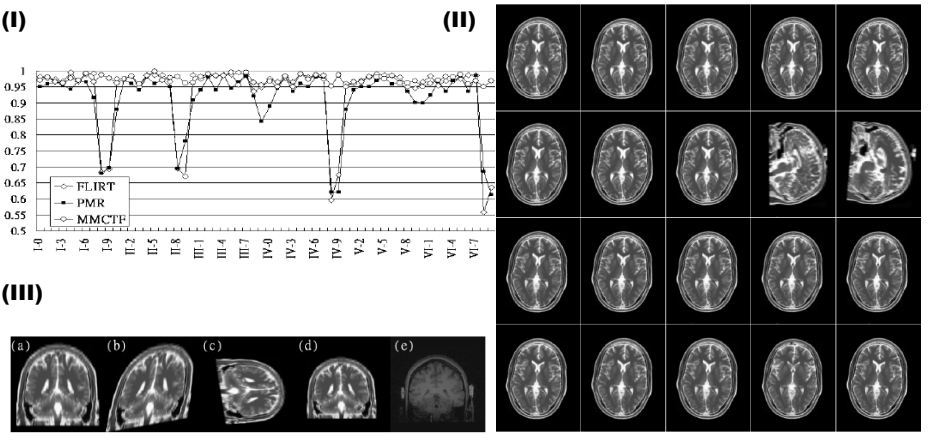

Fig. 6. (I) Normalized correlation between registered images with different initial transformations and the registered image without initial transformation. 6 cases (I~VI) in total and each with 10 different initial transformations (0~9). (II) The first two rows: Registration results of the same image with different initial transformations by FLIRT. The last two rows: Same results by MMCTF. 10 initial parameters from left to right, top to down are global scalings: 0.7, 0.8, 0.9, and 1.1, rotation about y-axis, 2, -2, 10, and -10 degrees, and rotation of -10 and 10 degrees plus 2nd skew factor = 0.4. (III) (a): Floating image; (b): (a) after initial transformation, rotation = -10 and 2nd skew factor = 0.4. (e): Reference image; (c): Result of registering (b) to (e) by FLIRT; (d): Result of registering (b) to (e) by MMCTF.

FLIRT and PMR fail to register some images correctly after large initial transformations. On the contrary, the MMCTF algorithm always gets consistent and good registration results throughout the experiments. Fig. 6 (II) shows one sample of the registration results obtained by FLIRT and MMCTF. While FLIRT fails to register the images in the last two cases, all results registered by the proposed MMCTF algorithm are very consistent. Fig. 6 (III) illustrates the coronal view. The floating image is first transformed by -10 degrees about the *y* axis and 0.4 of the second skew parameter.

4 Summary and Conclusion

In this paper, we try to improve the accuracy and robustness of biomedical image registration using a novel coarse-to-fine image registration framework. The results show that by integrating the novel multi-scale idea into original multi-resolution registration framework, we can improve both consistency and accuracy of both inter-modal and intra-modal registrations on 3D brain MR images. The proposed framework is also expected to be useful for registration of other types of biomedical images and may also contribute to high dimensional non-linear warping, which normally requires much more computation. Although the computation overhead of the TV-L^1 model on 3D data is high, it is fully parallel computable, which greatly alleviates this problem. Our future work includes comparing our method with other famous works such as mutual information based methods [14, 19] and extending the capability of our model to handle local affine transformation.

References

1. F. Alizadeh, and D. Goldfarb. “Second-order cone programming” Mathematical Programming 95(1), pp. 3-51, 2003.
2. S. Alliney “Digital filters as absolute norm regularizers” IEEE Trans. on Signal Processing, vol. 40, pp. 1548-1562, 1992.
3. T. F. Chan, and S. Esedoglu, “Aspects of Total Variation Regularized L1 Function Approximation” UCLA CAM Report 04-07, Feb, 2004.
4. T. Chen, W. Yin, X. S. Zhou, D. Comaniciu, T. S. Huang, “Illumination Normalization for Face Recognition and Uneven Background Correction Using Total Variation Based Image Models” CVPR, 2005.
5. D. Goldfarb, and W. Yin, “Second-order cone programming methods for total variation-based image restoration” Columbia CORC TR-2004-05, May, 2004.
6. M. Jenkinson, P. Bannister, J. M. Brady, and S. M. Smith, “Improved Optimisation for the Robust and Accurate Linear Registration and Motion Correction of Brain Images,” NeuroImage, 17(2), 825-841, 2002.
7. M. Jenkinson, P. Bannister, J. M. Brady, and S. M. Smith, “Improved Optimisation for the Robust and Accurate Linear Registration and Motion Correction of Brain Images,” NeuroImage, 17(2), 825-841, 2002.
8. R. K. -S. Kwan, A. C. Evans, and G. B. Pike, “MRI simulationbased evaluation of image-processing and classification methods”,IEEE Trans. Med. Img, 18(11):1085-1097, 1999.
9. J. B. A. Maintz and M. A. Viergever, “A survey of Medical Image Registration,” Medical Image Analysis, 2(1), 1-36, 1998.

10. Y. Meyer, “Oscillating patterns in image processing” Univ. Lecture Series 22, AMS, 2000.
11. M. Nikolova, “Minimizers of cost-functions involving nonsmooth data-fidelity terms” SIAM Journal on Numerical Analysis, vol. 40:3, pp. 965-994, 2002.
12. P. Oenev, and J. Atick, “Local feature analysis: A general statistical theory for object reperesentation” Network: Computation in Neural System, Vol. 7, pp. 477-500, 1996.
13. S. Osher, and O. Scherzer, “G-norm properties of bounded variation regularization” UCLA CAM Report 04-35, 2004. 13. W. Press, S. Teukolsky, W. Vetterling, and B. Flannery, “Numerical Recipies in C,” Cambridge University Press, 2nd Edition, 1995.
14. J.P.W. Pluim, J. B. A. Maintz, and M. A. Viergever, “Mutual information based registration of medical images: a survey”, IEEE Med. Img. 22:986-1004, 2003.
15. W. Press, S. Teukolsky, W. Vetterling, and B. Flannery, “Numerical Recipies in C,” Cambridge University Press, 2nd Edition, 1995.
16. A. Roche, G. Malandain, X. Pennec, and N. Ayache, “The corrlation ratio as a new similarity measure for multi-modal image registration,” MICCAI, 1998.
17. L. Rudin, S. Osher, and E. Fatemi, “Nonlinear total variation based noise removal algorithms” Physica D, vol. 60, pp. 259- 268, 1992.
18. D. Strong, and T. Chan, “Edge-preserving and scaledependent properties of total variation regularization” Inverse problems 19, pp.S165-S187, 2003.
19. P. Viola, and W. Wells, “ Alignment by maximization of mutual information” ICCV, 1995.
20. R. Woods, J. Mazziotta, and S. Cherry, “MRI-PET registration with automated algorithm,” Journal of Computer Assisted Tomography, 17(4), pp. 536-546, 1993.
21. W. Yin, T. Chen, X.-S. Zhou, and A. Chakraborty, “Background correction for cDNA microarray images using the TV+L1 model”, Bioinformatics, 21(10), pp 2410-2416, 2005.